ingegneria sismica
International Journal of Earthquake Engineering
Anno XLIII - Num. 3 - 2026

Development of a Multi-Scale Modeling and AI-Based Prediction and Risk Assessment Model for Earthquake Damage in Masonry Structures

Yinghao Xu[1,*]

[1] College of Civil Engineering, Xi'an University of Architecture and Technology 710055, Xian, China

SUMMARY: *This paper employs multi-scale modeling techniques integrated with computer vision damage detection to achieve automated identification and precise classification of seismic damage characteristics in masonry structures. The multi-scale modeling approach encompasses micro-unit modeling, multi-level modeling, and composite simulation modeling, effectively capturing the complex failure mechanisms of masonry structures during seismic events. Furthermore, the VGG16 neural network is employed for computer vision-based damage assessment. Transfer learning and data augmentation techniques enhance the model's universality and performance. Additionally, an AI-based risk assessment metric is established to quantitatively evaluate seismic damage in masonry structures by calculating structural response parameters and vulnerability coefficients. Results demonstrate robust performance across varying seismic intensities, maintaining an accuracy of 0.82 with a standard deviation of 0.025 under severe earthquake conditions, indicating high stability and reliability.*

KEYWORDS: *multiscale modeling; computer vision; masonry structures; risk assessment*

1 Introduction

Following an earthquake, buildings often sustain varying degrees of structural damage. Beyond those structures that collapse directly due to seismic activity, numerous buildings remain damaged yet temporarily maintain an appearance of stability. However, this "stability" becomes exceptionally fragile under the continuous impact of aftershocks, posing an imminent risk of collapse. This latent risk of collapse could very likely lead to more severe casualties and property losses [1]. Residents in disaster-stricken areas, lacking professional safety assessment knowledge and necessary evaluation tools, find it difficult to accurately judge the structural safety of their homes on their own. Consequently, they struggle to decide whether to evacuate potentially hazardous dwellings [2]. Among various building structures, masonry construction is widely favored and extensively used due to its advantages: readily available materials, low cost, rapid construction, and excellent thermal insulation [3]. Therefore, accurately assessing the post-earthquake safety of masonry structures is an urgent practical necessity [4]. However, in post-earthquake emergencies, particularly at disaster sites, time is of the essence, demanding rapid assessment of building damage levels. The challenge lies in the fact that conducting structural safety evaluations for each building in a large-scale damaged complex requires a substantial number of assessors and is time-consuming.

Cattari, S. and Angiolilli, M. compared the limitations of current definitions and

*yinghaoxu0120@xauat.edu.cn
https://doi.org/10.65102/is20261197 Published: 10 June, 2026

assessment methodologies for structural damage in non-masonry buildings. They proposed a comprehensive definition of damage at the structural level that considers overall behavior characteristics while accounting for failure modes occurring in individual structural elements such as piers, wing walls, and floor slabs [5]. Lourenço, P. B. et al. combined finite element method (FEM) and digital elevation model (DEM) to represent masonry material at scale, while using flowchart code components for representation to clarify data relationships. This method enhances computational efficiency while performing seismic assessments of masonry structures [6]. Bhatia, M. et al. developed a comprehensive earthquake prediction framework using artificial intelligence. By extracting data features through IoT-edge computing and employing a prototype architecture to collect real-time IoT data, the model demonstrated high performance in classification accuracy, prediction efficiency, computational latency, reliability, and stability [7]. Lu, X et al. summarized AI applications in earthquake and structural engineering, including seismic ground motion analysis, structural engineering computation methods, structural system identification and damage monitoring, and seismic structural control. These findings fully validate AI's critical role in earthquake analysis [8]. Dong, Z. Q. et al. analyzed the impact of scouring on seismic performance using single-story masonry structures as a case study. Considering disaster risk and structural vulnerability, they examined structural failure mechanisms based on risk assessment theory and reliability metrics [9]. D'Amato, M. et al. incorporated a sample of 58,323 masonry buildings into their study, examining damage observed after the 2009 L'Aquila earthquake on April 6. They derived vulnerability curves using a decay method to analyze seismic risk and vulnerability levels [10]. Riga, E. et al. highlighted that the accuracy of seismic risk model predictions is influenced by multiple factors. This study introduced a method for validating seismic risk models and summarized uncertainty factors affecting prediction outcomes, providing reference for seismic risk assessment research [11]. Shendkar, M. R. et al. proposed an Earthquake Damage Risk Index (EDRI) optimization method to investigate damage conditions of RC buildings in the Koina-Vana region. The study emphasized that seismic retrofitting measures should be prioritized in the study area to reduce post-earthquake casualties and damage to buildings and facilities [12].

While current research focuses extensively on earthquake damage prediction and risk assessment, the rapid advancement of artificial intelligence (AI) provides a robust foundation for deeper exploration of structural characteristics and earthquake damage forecasting. This paper employs multiscale modeling and artificial intelligence (AI) to construct a multiscale-AI coupled model for calculating damage indices and evaluating overall structural safety. By incorporating computer vision for damage detection, seismic damage characteristics can be extracted more effectively, enhancing assessment accuracy and efficiency. This establishes risk assessment metrics to meet the urgent need for rapid post-earthquake response.

2 Multi-scale modeling

2.1 Definition of Earthquake Damage

Structural damage under seismic loading is primarily categorized into geometric damage and mechanical damage. After experiencing an earthquake, the strength of masonry materials and mortar interfaces undergoes a certain degree of reduction, altering their performance during aftershocks. Currently, it is challenging to provide an appropriate definition and description for this phenomenon [13]. Following an earthquake, the degradation of mechanical properties has a relatively minor impact on the load-bearing capacity of masonry structures.

Consequently, the effects of material damage on mechanical performance reduction are no longer considered in seismic damage simulations for masonry structures [14, 15]. Therefore, this paper defines structural damage under seismic loading solely based on geometric damage, disregarding mechanical performance degradation at the material level.

By summarizing and analyzing seismic damage data, we identify crack development, block displacement, and localized failure in masonry structures. Assuming post-earthquake damage occurs at masonry walls and window partition walls, seismic damage to masonry structures is defined as combinations of cracks and cracks + spalling. Damage parameters are shown in Table 1, with the height of cracks + spalling set at 180 mm. The geometric characteristics of cracks are represented by crack width w, crack length l, and crack depth d. The geometric characteristics of spalling are represented by spalling thickness a, spalling height h', and spalling width b. Due to varying cross-sectional dimensions of masonry walls, relative values are employed when selecting specific dimensions: relative crack length $l/h=0.5$, relative crack depth $d/h=0.05$, relative spalling height $h'/h=0.3$, and relative spalling width $b/h=0.2$.

Table 1: Injury Parameters

Injury Type	w /mm	l /mm	d /mm	a /mm	b /mm	h' /mm
Crack	2	300	30	0	0	0
Crack + Spalling	2	300	30	20	10	180

2.2 Model Design and Development

In the computational model, wall thickness and material parameters are as shown in Table 2. Masonry wall materials consist of MU10 and MU7.5 standard fired bricks, with mortar strength grades of M5 and M7.5. Wall thickness is 240 mm, while non-load-bearing partition walls are 120 mm thick. Floor dead load (4.0 kN/m²) + live load (2.0 kN/m²). Based on varying seismic intensities, representative vulnerable sections of the ground-floor exterior walls and window partition walls were selected for analysis [16].

Table 2: Wall Thickness and Material Parameters

Component Type	Thickness/ mm	Material	Strength Grade	Standard
Load-bearing Wall	240	Fired Common Brick	MU10	M5 Mortar
Non-load-bearing Wall	120	Fired Common Brick	MU7.5	M5 Mortar
Structural Column	240×240	Concrete	C25	Reinforcement 4Φ12
Lintel	240×180	Concrete	C25	Reinforcement 4Φ10

When establishing finite element models, Figure 1 depicts a micro-element model, with a full micro-element model serving as a reference model [17].

Figure 1: Microscopic Unit Model

Figure 2 depicts a multiscale model. When employing multiscale modeling, a microscopic model is established for the locations where cracks appear, along with node sections and micro-mechanisms such as brick misalignment, represented by solid elements [18]. The remaining wall and floor sections are modeled using a macroscopic approach, represented by beam elements.

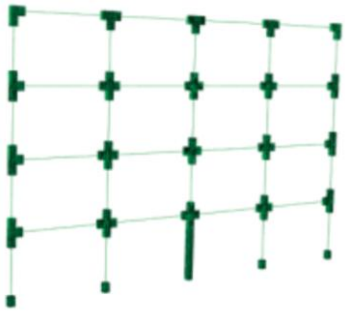

Figure 2: Multi-scale Model

Figure 3 shows the hybrid simulation model. The test sub-structure is depicted in Figure 3(a). During hybrid simulation for seismic damage prediction and risk assessment, critical vulnerable sections are modeled separately as the test sub-structure. The numerical sub-structure is shown in Figure 3(b), with the remaining portions modeled as the numerical sub-structure.

(a) Test Substructure

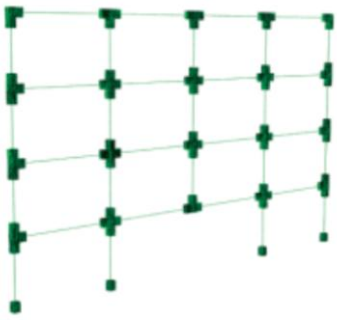

(b) Numerical Substructure

Figure 3: Hybrid Simulation Model

2.3 Structural Response Indicators

2.3.1 Definition of Structural Damage

Since masonry structures tend to produce unrecoverable lateral displacements u_r after experiencing strong seismic actions, in order to take into account the effect of u_r on structural damage, the starting displacement point of the restoring force-displacement curve of the damaged structure is designated as u_r, and the end point remains as u_u [19, 20]. The area enclosed by the restoring force-displacement curve of the structure under unidirectional horizontal loading after the earthquake is S'', whose physical significance is the ability of the damaged structure to dissipate the strain energy under unidirectional horizontal loading with:

$$S' = S - S'' \tag{1}$$

Here, S denotes the capacity of an undamaged structure to dissipate plastic strain energy and store elastic strain energy under unidirectional horizontal loading.

If damage to masonry structures under seismic action is defined as the loss of the structure's capacity to dissipate plastic strain energy and store elastic strain energy under unidirectional horizontal loading, then the damage index D_I is:

$$D_I = S'/S = 1 - S''/S \tag{2}$$

2.3.2 Calculation of Damage Indicators

Based on the definition of structural damage, the damage model is obtained:

$$D_I = D_R + D_H \tag{3}$$

For “displacement-first failure” caused by inter-story drift exceeding limits, $D_I = D_R = 1$ holds. For “cumulative damage failure” induced by low-cycle repeated loading, the lateral stiffness and load-bearing capacity of masonry structures are significantly reduced, yielding:

$$D_R = \begin{cases} S_R / S, & u_{max} < u_u \\ 1, & u_{max} \geq u \end{cases}; D_H = \frac{S_h}{S} \tag{4}$$

The model is applicable to single-degree-of-freedom equivalent systems of masonry structures, as well as to scenarios where unidirectional horizontal loads are applied along the direction of irreversible deformation occurring in masonry walls post-earthquake [21].

2.3.3 Simplification of Damage Calculation

The inter-story recovery force and inter-story lateral displacement relationship curve of masonry structures is simplified to a bilinear relationship of an ideal elastoplastic body, where F_y and F_{dy} represent the lateral resistance of the undamaged and damaged structures, respectively. u_y and u_{dy} denote the yield displacements for the undamaged and damaged structures, respectively. The following relationship holds:

$$K = F_y / u_y, K_d = F_{dy} / u_{dy} \tag{5}$$

K, K_d represents the lateral stiffness of the undamaged structure and the damaged structure, respectively. According to the aforementioned damage definition, we have:

$$D_I = 1 - \frac{S''}{S} = 1 - \frac{F_{dy}\left(u_u - u_r - 0.5u_{dy}\right)}{F_y\left(u_u - 0.5u_y\right)} \tag{6}$$

Order:

$$\mu_u = u_u / u_y, \mu_r = u_r / u_y \tag{7}$$

Then there is:

$$D_I = 1 - \frac{F_{dy}}{F_y} \cdot \frac{\mu_u - \mu_r - 0.5\frac{u_{dy}}{u_y}}{\mu_u - 0.5} \tag{8}$$

Order:

$$\xi_F = F_{dy} / F_y, \xi_K = K_d / K \tag{9}$$

Then there is:

$$D_I = 1 - \frac{\xi_F\left(\mu_u - \mu_r - 0.5\frac{\xi_F}{\xi_K}\right)}{\mu_u - 0.5} (D_I > 1 \; or \; D_I = 1) \tag{10}$$

$$D_R = \frac{\mu_r}{\mu_u - 0.5}, D_H = D_I - D_R \tag{11}$$

where: μ_u denotes the ductility coefficient for ultimate inter-story displacement of masonry structures, μ_r denotes the ductility coefficient for irreversible inter-story displacement of the structure, ξ_F denotes the residual strength coefficient of the structure, and ξ_K denotes the residual stiffness coefficient of the structure. Equations (9)–(11) indicate that the seismic damage index of masonry structures is primarily influenced by the structure's irreversible displacement, strength damage, and stiffness damage, in addition to its ultimate displacement ductility coefficient.

3 AI Risk Assessment Model Development

3.1 Computer Vision Damage Detection

In the context of artificial intelligence, image classification techniques in computer vision have received extensive research and application, particularly in scenarios where data annotation is challenging and datasets are limited. These techniques enable the full utilization of limited labeled samples to enhance model generalization capabilities and performance [22]. For masonry structures exhibiting concurrent spalling and cracking damage due to seismic impact, to effectively capture damage information, the damage segmentation results from all

sub-images are overlaid to yield comprehensive damage information at the pixel level. The collected raw images undergo matrix padding before being sliced into a set of 224×224 sub-images in a row-by-row, column-by-column manner without overlap. These sub-images are then fed into the damage classification model. The first-level classifier within the classification module determines whether each sub-image contains damage. If the first-level classifier outputs a damaged sub-image, the corresponding sub-image is passed to the second-level classifier for further damage type identification.

The classification network employs the VGG16 architecture. Figure 4 depicts the VGG16 classifier model, which consists of 13 convolutional layers, 3 fully connected layers, and a softmax output layer. Layers are separated by max-pooling operations. The network employs multiple smaller 3×3 convolutional kernels instead of a single larger kernel. This approach reduces parameters while effectively performing more nonlinear mappings, thereby enhancing the network's fitting or expressive capabilities. Training a model from scratch requires substantial data and computational resources. Researchers often employ transfer learning to rapidly adapt pre-trained networks to specific task domains. The combination of convolutional and pooling layers is commonly used for feature extraction, while fully connected layers perform feature integration and category classification. Therefore, this paper utilizes the VGG16 model pre-trained on the ImageNet dataset. During model fine-tuning, the first 13 convolutional layers of VGG16 were frozen to preserve the original image feature extraction method. Global average pooling layers connect the convolutional layers to five custom fully connected layers. To mitigate overfitting, data augmentation techniques such as image scaling, translation, and flipping were employed. The classification network was trained using SGD as the optimizer. The initial learning rate is set to 0.0001, the momentum parameter is set to 0.9, and the learning rate decay value after each update is set to le-6. The loss function uses categorical_crossentropy, the batch size is set to 32, and the number of iterations is set to 100.

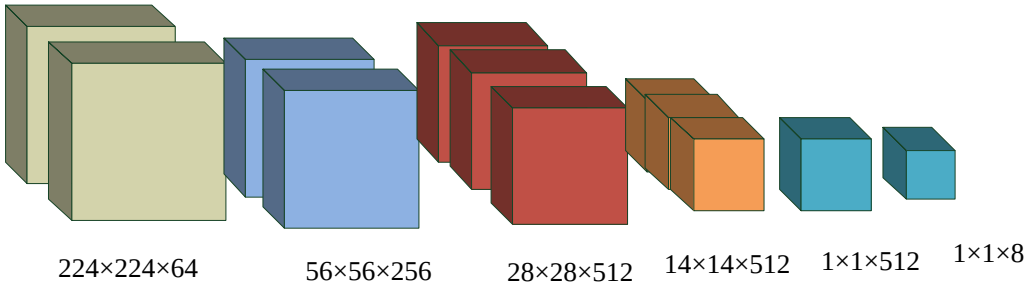

Figure 4: VGG16 classifier model

The post-earthquake damage detection method for masonry structures proposed in this paper, based on the VGG16 classifier model, addresses issues such as the substantial workload of sample labeling and the lack of quantitative differentiation metrics for crack and spalling categories.

3.2 Risk Assessment Metrics

In a probabilistic sense, the values in the masonry structure matrix can be regarded as the probability-weighted representatives of the structure's vulnerability index across five damage states, corresponding to probability distributions ranging from 0.00–0.20, 0.20–0.40, 0.40–0.60, 0.60–0.80, and 0.80–1.00. This yields Equation (12):

$$P(\textit{Destruction state}) = P\left(x + \frac{1}{2}\Delta x\right) - P\left(x - \frac{1}{2}\Delta x\right) = f(x)\Delta x \tag{12}$$

In the formula: P represents the probability value, derived from the percentage of masonry structures entering a certain state of damage under a specific intensity or peak acceleration during computer vision detection. x denotes the vulnerability index, taken as 0.1, 0.3, 0.5, 0.7, and 0.9. Δx represents the interval length, with each interval set at 0.2, and $f(x)$ denotes the probability density function. When x takes values of 0.1, 0.3, 0.5, 0.7, and 0.9, $f(x)$ corresponds to the probability density values for the five damage states, respectively. After calculating structural response indicators via multiscale modeling, computer vision is employed to detect masonry damage. Table 3 presents the probability density matrix for vulnerability indices. Values of 0.1, 0.3, 0.5, 0.7, and 0.9 correspond to five states: fundamentally intact, minor damage, moderate damage, severe damage, and collapse, respectively. Sa denotes spectral acceleration.

Table 3: Probability density matrix of damage index

Sa(0.25)(g) interval	0.1	0.3	0.5	0.7	0.9
Sa<0.02	5	0	0	0	0
0.02≤Sa<0.05	4.85	0.15	0	0	0
0.05≤Sa<0.10	2.4	2	0.55	0.05	0
0.10≤Sa<0.25	0.1	2.3	1.85	0.7	0.05
Sa≥0.25	0	0.1	1.05	2.75	1.1

4 Analysis of Model Construction Results

4.1 Dataset and Operating Condition Design

4.1.1 Simulated Data

At the macro scale, the masonry structure is analyzed as a whole, describing its overall mechanical response based on wall thickness and material parameters. At the micro-scale, nonlinear interface effects between brick units and mortar layers are considered. Interface elements simulate damage evolution behaviors such as cracking, slippage, and debonding, thereby reflecting the complex failure mechanisms of masonry under seismic loading. Boundary conditions are set as fixed at the bottom and free at the top, with loading applied as unidirectional horizontal seismic input, accurately representing lateral force characteristics under seismic action.

For seismic input, representative earthquake records were selected, including internationally recognized classic seismic data such as the El Centro wave and Taft wave. These were combined with actual seismic records released by the China Earthquake Networks Center to ensure diversity and regional applicability of the seismic input samples. By varying the peak ground acceleration (PGA) and characteristic period of the input seismic motions, multiple simulated scenarios were constructed to cover a range of intensities from minor to major earthquakes.

4.1.2 Data Partitioning

The dataset was split into a training set (70%), validation set (15%), and test set (15%). This

allocation ensures the model receives sufficient training while retaining adequate samples for performance evaluation. To prevent overfitting, data augmentation techniques were employed. This involved randomly modifying the amplitude and period of seismic motions to enrich data diversity, thereby enhancing the model's robustness and generalization capabilities.

4.2 Analysis of Comparison Results

4.2.1 Vulnerability Comparison

To further validate the model's applicability across the full range of intensities, seismic motion inputs with different peak accelerations were selected. The seismic damage probabilities predicted by the three methods were statistically analyzed and compared with the results from actual seismic damage surveys. Damage levels were categorized into four grades: Minor (S1), Moderate (S2), Severe (S3), and Collapse (S4). The comparison focused on the performance of different methods for moderate and severe damage, as these categories best reflect differences in structural seismic performance.

Table 4 shows the predicted seismic damage probabilities for the three methods under different PGA levels. At low intensity (PGA=0.1g), the measured value was 0.62. The pure AI model overestimated DS1 at 0.7 but underestimated DS2 and DS3 probabilities. This indicates that pure AI is overly sensitive to minor damage under weak seismic conditions while struggling to accurately distinguish moderate and severe damage. Finite element analysis (FEA) predictions align more closely with actual measurements than the models proposed in this paper, indicating that physical constraints retain advantages for low-intensity prediction. At moderate intensity (PGA=0.3g), the multiscale modeling + AI model closely matches actual damage levels across all categories, particularly for DS2 and DS3, with predicted values of 0.24 and 0.09 respectively, approaching actual values. At high intensities (PGA=0.5g), FEA predictions showed a significantly higher proportion of severe damage. For DS3, the predicted value was 0.35 compared to the measured value of 0.28, indicating an overestimation of damage under strong earthquakes. Overall, the proposed model delivered predictions closest to observed results, demonstrating highest agreement at DS3 and DS4 levels. The multiscale modeling coupled with AI effectively addressed limitations of both approaches, showcasing potential for rapid post-earthquake damage assessment and urban risk analysis.

Table 4: Damage probability predicted by three methods under different PGAs

PGA	Method	DS1	DS2	DS3	DS4
0.1g	Actual measurement	0.62	0.25	0.1	0.03
	FEA	0.59	0.28	0.11	0.02
	AI	0.7	0.2	0.07	0.03
	Multi-scale modeling + AI	0.64	0.24	0.09	0.03
0.3g	Actual measurement	0.4	0.3	0.2	0.1
	FEA	0.35	0.33	0.25	0.07
	AI	0.46	0.32	0.15	0.07
	Multi-scale modeling + AI	0.41	0.31	0.21	0.09
0.5g	Actual measurement	0.25	0.28	0.28	0.19
	FEA	0.18	0.29	0.35	0.18
	AI	0.32	0.3	0.22	0.16
	Multi-scale modeling + AI	0.26	0.27	0.29	0.18

4.2.2 Prediction Accuracy and Residual Analysis

Using the test set data, the prediction errors of the three methods were calculated for three metrics: interlayer displacement angle (IDR), energy dissipation (E), and damage index (DI). Root mean square error (RMSE) and mean absolute error (MAE) were adopted as evaluation indicators. Table 5 compares prediction errors across different seismic damage indices. Experimental results indicate that for IDR prediction, the multi-scale modeling + AI approach achieves RMSE = 0.021 and MAE = 0.014, significantly outperforming both FEA (RMSE = 0.028, MAE = 0.019) and AI (RMSE = 0.031, MAE = 0.022). This indicates that the proposed model better captures the deformation characteristics of masonry structures under varying seismic intensity levels. For energy dissipation (E), the Hybrid model achieved RMSE=2.31 MJ and MAE=1.62 MJ, compared to FEA's 2.89 MJ and 1.95 MJ, and AI's 3.24 MJ and 2.18 MJ. This demonstrates that multiscale modeling significantly enhances fitting capability for energy dissipation—a metric closely tied to nonlinear energy dissipation mechanisms. The superiority of this model is particularly evident in predicting the Damage Index (DI). Its MAE=0.13 is markedly lower than FEA=0.16 and AI=0.19, while its RMSE reaches 0.18, compared to FEA=0.22 and AI=0.25. This result indicates that the hybrid model more accurately reflects the actual damage severity when quantifying overall earthquake damage.

Table 5: Comparison of prediction errors under different earthquake damage indicators

Index	Method	RMSE	MAE
Interstory drift angle (IDR)	FEA	0.028	0.019
	AI	0.031	0.022
	Multi-scale modeling + AI	0.021	0.014
Energy dissipation (E, MJ)	FEA	2.89	1.95
	AI	3.24	2.18
	Multi-scale modeling + AI	2.31	1.62
Damage Index (DI)	FEA	0.22	0.16
	AI	0.25	0.19
	Multi-scale modeling + AI	0.18	0.13

4.2.3 Computational Efficiency Comparison

On the same hardware platform (Intel i7 CPU + RTX 3090 GPU), the average computation time required for 100 seismic simulation predictions using the three methods is shown in Figure 5. FEA took the longest per simulation with significant variability, ranging from 60 to 82 seconds, indicating high resource consumption and strong hardware dependency during multiple simulations. The model proposed in this paper exhibits minimal variation, ranging from 0.5 to 1.2 seconds, demonstrating exceptional efficiency in single-run predictions. The AI model's processing time falls between the two approaches, slightly slower than the multiscale-AI method but significantly faster than FEA, achieving a balanced trade-off between computational accuracy and efficiency.

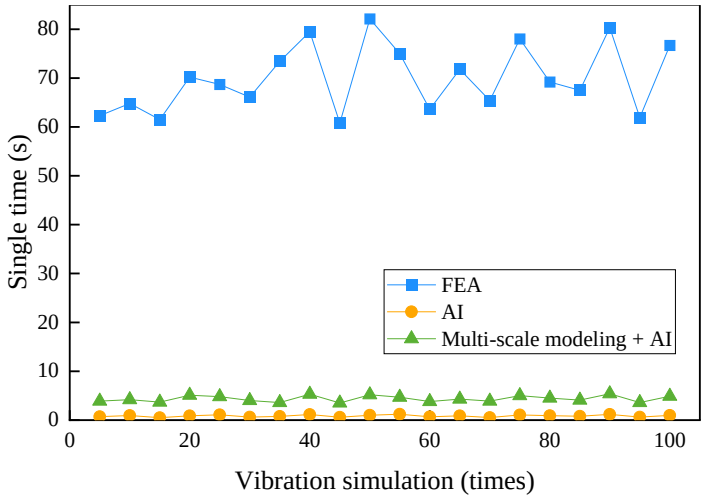

Figure 5: Comparison of computational efficiency

4.2.4 Robustness Test Results

Selecting strong-motion (PGA=0.4g, 0.5g) and weak-motion (PGA=0.05g, 0.1g) seismic input data, we analyzed the stability of three methods in predicting earthquake damage levels. The robustness test results are shown in Table 6. Under weak-motion conditions, the accuracy differences among the three methods were negligible. However, under strong seismic conditions, the accuracy of the FEA and pure AI models decreased significantly. Notably, the pure AI model's accuracy dropped from 0.85 to 0.68, demonstrating poor robustness. In contrast, the accuracy of the proposed model remained at 0.82, indicating it maintains high reliability under strong seismic conditions. The standard deviation results also show that the proposed model is the most stable (STD=0.025).

Table 6: Robustness test results

Method	Weak earthquake accuracy	Strong earthquake accuracy	STD
FEA	0.81	0.76	0.035
AI	0.85	0.68	0.085
Multi-scale modeling + AI	0.87	0.82	0.025

5 Discussion

This study developed a method for predicting and evaluating seismic damage in masonry structures by integrating multi-scale modeling and artificial intelligence, proposing structural response indicators and an AI risk assessment model. However, the research still has areas for improvement, specifically:

(1) Damage mechanisms such as post-earthquake longitudinal and transverse tensile failure, localized crushing of walls beneath beams, and significant deflection of lintels require further investigation to ensure a more comprehensive assessment of overall structural safety. [23].

(2) Although data augmentation yielded a dataset largely meeting training requirements, AI still faces challenges due to relatively insufficient sample size. When feasible, further collection of masonry structural damage images is recommended to enhance sample diversity and ensure the model learns broader damage characteristics.

(3) This study offers a new feasible approach for quantifying “crack” and “spalling” parameters. However, limitations in data sources constrain the determination of precise proportional factors. Future research will further examine how factors like shooting distance and angle affect parameter characteristics, thereby enhancing the accuracy and reliability of parameter quantification.

(4) Future research will focus on holistic structural analysis to achieve automated structural safety assessment independent of manual intervention. This will involve comprehensively considering multiple damage scenarios in structural components to address challenges and limitations that may arise from diverse data sources and practical application scenarios.

6 Conclusion

This paper employs a multi-scale-AI hybrid model to predict and accurately evaluate seismic damage in masonry structures. Experimental results demonstrate that this model outperforms both traditional finite element analysis (FEA) and AI models across multiple key metrics. The model completes single simulations within 0.5–1.2 seconds, significantly faster than standalone AI models. For the three metrics—Interstory Drift Ratio (IDR), Energy Dissipation (E), and Damage Index (DI)—this model outperforms both FEA and pure AI models. Notably, in predicting DI, the Mean Absolute Error (MAE) of this model is 0.13, compared to 0.16 for FEA and 0.19 for AI. Moreover, the model demonstrated robust performance across varying earthquake intensities. Even under strong seismic conditions, its accuracy remained at 0.82 with a standard deviation of 0.025, proving high stability and reliability. Future work will focus on refining the model, expanding sample diversity, and enhancing the accuracy and reliability of parameter quantification to ultimately achieve fully automated building safety assessment.

Funding

This work was supported by 2019YFC15090302.

Author's Profile

Yinghao Xu was born in Xian，Shanxi. China, in 1995. He earned his bachelor's degree from Beijing Jiaotong University and a master's from the University at Buffalo SUNY in the United States. He is currently studying at the School of Civil Engineering of Xi'an University of Architecture and Technology. His primary research focus is on the seismic performance of masonry structures with bottom frames.

References

[1] Hulsey, A. M., Galvis, F. A., Baker, J. W., & Deierlein, G. G. (2024). Elevated collapse risk based on decaying aftershock hazard and damaged building fragilities. *Earthquake Spectra*, 40(1), 674-704.

[2] Lulić, L., Ožić, K., Kišiček, T., Hafner, I., & Stepinac, M. (2021). Post-earthquake damage assessment—Case study of the educational building after the Zagreb

earthquake. *Sustainability,* 13(11), 6353.

[3] Tsiavos, A., Sextos, A., Stavridis, A., Dietz, M., Dihoru, L., Di Michele, F., & Alexander, N. A. (2021). Low-cost hybrid design of masonry structures for developing countries: Shaking table tests. *Soil Dynamics and Earthquake Engineering,* 146, 106675.

[4] Hafner, I., Lazarević, D., Kišiček, T., & Stepinac, M. (2022). Post-Earthquake assessment of a historical masonry building after the Zagreb earthquake—case study. Buildings, 12(3), 323.

[5] Cattari, S., & Angiolilli, M. (2022). Multiscale procedure to assign structural damage levels in masonry buildings from observed or numerically simulated seismic performance. *Bulletin of Earthquake Engineering,* 20(13), 7561-7607.

[6] Lourenço, P. B., Funari, M. F., & Silva, L. C. (2022). Building resilience and masonry structures: How can computational modelling help?. *Computational modelling of concrete and concrete structures,* 30-37.

[7] Bhatia, M., Ahanger, T. A., & Manocha, A. (2023). Artificial intelligence based real-time earthquake prediction. *Engineering Applications of Artificial Intelligence,* 120, 105856.

[8] Lu, X., Plevris, V., Tsiatas, G., & De Domenico, D. (2022). Artificial intelligence-powered methodologies and applications in earthquake and structural engineering. *Frontiers in Built Environment,* 8, 876077.

[9] Dong, Z. Q., Li, G., Song, B., Lu, G. H., & Li, H. N. (2022). Failure risk assessment method of masonry structures under earthquakes and flood scouring. *Mechanics of Advanced Materials and Structures,* 29(21), 3055-3066.

[10] D'Amato, M., Laguardia, R., Di Trocchio, G., Coltellacci, M., & Gigliotti, R. (2022). Seismic risk assessment for masonry buildings typologies from L'Aquila 2009 earthquake damage data. *Journal of earthquake engineering,* 26(9), 4545-4579.

[11] Riga, E., Karatzetzou, A., Apostolaki, S., Crowley, H., & Pitilakis, K. (2021). Verification of seismic risk models using observed damages from past earthquake events. *Bulletin of Earthquake Engineering,* 19(2), 713-744.

[12] Shendkar, M. R., Pradeep Kumar, R., Mandal, S., Maiti, P. R., & Kontoni, D. P. N. (2021). Seismic risk assessment of reinforced concrete buildings in Koyna-Warna region through EDRI method. *Innovative Infrastructure Solutions,* 6(3), 141.

[13] Zhao, Z., Cui, J., Liu, C., Liu, H., ur Rehman, M., Chen, W., & Peng, Z. (2023). Seismic damage characteristics of large-diameter shield tunnel lining under extreme-intensity earthquake. *Soil Dynamics and Earthquake Engineering,* 171, 107958.

[14] Hoveidae, N., Fathi, A., & Karimzadeh, S. (2021). Seismic damage assessment of a historic masonry building under simulated scenario earthquakes: A case study for Arge-Tabriz. *Soil Dynamics and Earthquake Engineering,* 147, 106732.

[15] Saviano, F., Parisi, F., & Lignola, G. P. (2022). Material aging effects on the in-plane

lateral capacity of tuff stone masonry walls: A numerical investigation. *Materials and Structures*, 55(7), 198.

[16] Wang, Z., Li, B., & Liang, X. (2022). Utilization of river sediment, sewage sludge and wheat straw as the primary raw material in sintered-shale bricks. *Journal of Material Cycles and Waste Management*, 24(6), 2401-2415.

[17] Guan, M., Hang, X., Wang, M., Zhao, H., Liang, Q. Q., & Wang, Y. (2024). Development and implementation of shear wall finite element in OpenSees. *Engineering Structures*, 304, 117639.

[18] Nguyen, T. K., Desrues, J., Vo, T. T., & Combe, G. (2022). FEM× DEM multi-scale model for cemented granular materials: Inter-and intra-granular cracking induced strain localisation. *International Journal for Numerical and Analytical Methods in Geomechanics*, 46(5), 1001-1025.

[19] Zhang, Y., Wang, Z., Jiang, L., Skalomenos, K., & Zhang, D. (2023). Seismic fragility analysis of masonry structures considering the effect of mainshock-aftershock sequences. *Engineering Structures*, 275, 115287.

[20] Kocaman, İ. (2023). The effect of the Kahramanmaraş earthquakes (Mw 7.7 and Mw 7.6) on historical masonry mosques and minarets. *Engineering Failure Analysis*, 149, 107225.

[21] Sarhosis, V., Dais, D., Smyrou, E., Bal, I. E., & Drougkas, A. (2021). Quantification of damage evolution in masonry walls subjected to induced seismicity. *Engineering Structures*, 243, 112529.

[22] Zhang, Y., & Yuen, K. V. (2022). Review of artificial intelligence-based bridge damage detection. *Advances in Mechanical Engineering*, 14(9), 16878132221122770.

[23] Quaranta, G., Angelucci, G., & Mollaioli, F. (2022). Near-fault earthquakes with pulse-like horizontal and vertical seismic ground motion components: Analysis and effects on elastomeric bearings. *Soil Dynamics and Earthquake Engineering*, 160, 107361.